PHYSICAL REVIEW B **97**, 064514 (2018)

Superconductivity in pressurized $CeRhGe_3$ and related noncentrosymmetric compounds

Honghong Wang,[1,3] Jing Guo,[1] Eric D. Bauer,[2] Vladimir A. Sidorov,[4] Hengcan Zhao,[1,3] Jiahao Zhang,[1,3] Yazhou Zhou,[1]
Zhe Wang,[1,3] Shu Cai,[1,3] Ke Yang,[5] Aiguo Li,[5] Xiaodong Li,[6] Yanchun Li,[6] Peijie Sun,[1] Yi-feng Yang,[1,3] Qi Wu,[1]
Tao Xiang,[1,3] J. D. Thompson,[2,*] and Liling Sun[1,3,†]
[1]*Institute of Physics, National Laboratory for Condensed Matter Physics, Chinese Academy of Sciences, Beijing 100190, China*
[2]*Los Alamos National Laboratory, MS K764, Los Alamos, New Mexico 87545, USA*
[3]*University of Chinese Academy of Sciences, Beijing 100190, China*
[4]*Institute for High Pressure Physics, Russian Academy of Sciences, 142190 Troitsk, Moscow, Russia*
[5]*Shanghai Synchrotron Radiation Facilities, Shanghai Institute of Applied Physics, Chinese Academy of Sciences, Shanghai 201204, China*
[6]*Institute of High Energy Physics, Chinese Academy of Science, Beijing 100049, China*

(Received 19 August 2017; revised manuscript received 5 February 2018; published 20 February 2018)

We report the discovery of superconductivity in pressurized $CeRhGe_3$, a nonsuperconducting member of the isostructural family of noncentrosymmetric heavy-fermion compounds $CeTX_3$ (T = Co, Rh, Ir and X = Si, Ge). Superconductivity appears in $CeRhGe_3$ at a pressure of 19.6 GPa and the transition temperature T_C reaches a maximum value of 1.3 K at 21.5 GPa. This finding provides an opportunity to establish systematic correlations between superconductivity and material properties within this family. Though ambient-pressure unit-cell volumes and critical pressures for superconductivity vary substantially across the series, all family members reach a maximum $T_C^{\max}$ at a common (±1.7%) critical cell volume V_{crit}, and $T_C^{\max}$ at V_{crit} increases with increasing spin-orbit coupling strength of the d electrons. These correlations show that substantial Kondo and spin-orbit couplings favor superconductivity in this family, the latter reflecting the role of broken centrosymmetry.

DOI: 10.1103/PhysRevB.97.064514

I. INTRODUCTION

The discovery of the first heavy-fermion superconductor $CeCu_2Si_2$ in 1979 [1] opened the new field of unconventional superconductivity and posed a fundamental challenge for understanding the superconducting mechanism. After nearly 40 years, more than 40 heavy-fermion superconductors have been found, and there is growing appreciation that their superconductivity emerges at the border of competing or coexisting electronic orders [2], suggesting that fluctuations of these orders may be the source of superconductivity. Among heavy-fermion compounds, the $CeTX_3$ (T = Co, Ir, Rh and X = Si, Ge) [3,4] family belongs to a subset whose crystallographic structure ($I4mm$) lacks a center of inversion symmetry [5,6]. Except for the mixed-valence member $CeCoSi_3$, others of the family order antiferromagnetically at atmospheric pressure. Application of pressure to $CeRhSi_3$, $CeIrSi_3$, and $CeCoGe_3$, $CeIrGe_3$ suppresses their Néel temperature toward zero temperature where a dome of superconductivity emerges [7–18]. These observations have led to suggestions that magnetic fluctuations may induce unconventional superconductivity, but this remains unsettled, in part because of the possible nontrivial role of antisymmetric spin-orbit coupling that is a consequence of these materials' noncentrosymmetry [6]. Besides its possible role in forming superconductivity, sufficiently strong spin-orbit coupling would also lead to an unusual pairing state that is a mixture of spin-singlet and spin-triplet components.

As a member of the magnetic $CeTX_3$ family, $CeRhGe_3$ is expected to become superconducting under pressure. However, experiments to about 8 GPa find only a monotonic increase in its Néel temperature [15]. Here, we report an observation of pressure-induced superconductivity in $CeRhGe_3$. As will be discussed, this discovery allows a broader perspective on conditions favoring superconductivity in this family of nominally isoelectronic compounds.

II. EXPRIMENTAL DETAILS

Single crystals of $CeRhGe_3$ were grown from a $Rh_{0.25}Ge_{0.75}$ eutectic self-flux ($T_{\mathrm{melt}} = 850\,^{\circ}\mathrm{C}$) [19,20]. The elements Ce, Rh, Ge were arc melted together in a molar ratio of Ce : Rh : Ge = 1 : 3.5 : 13.5 (corresponding to $CeRhGe_6 + 10\,Rh_{0.25}Ge_{0.75}$) on a water-cooled copper hearth in an ultrahigh-purity Ar atmosphere. The arc-melted button was then placed in a 2-ml alumina crucible and sealed under vacuum in a silica tube. The tube was heated to 1150 °C, held at that temperature for 12 h, and then cooled slowly at 2 °C/h to 875 °C. The excess flux was removed by spinning the (inverted) silica tube in a centrifuge. Single crystals of $CeRhGe_3$ in the form of three-dimensional, tetrahedral-like blocks with well-defined facets and volumes ranging from 1 to 4 mm^3 were obtained.

High-pressure resistance and magnetoresistance measurements were carried out in a diamond-anvil cell made of a Be-Cu alloy. Diamond anvils with 300-μm flats were used for all high-pressure experiments. In the resistance measurements, NaCl powder was employed as the pressure-transmitting medium to obtain a quasihydrostatic pressure environment, which has

---

[*] jdt@lanl.gov

[†] llsun@iphy.ac.cn

been widely used for high-pressure transport measurements [21]. The four-probe method determined the *ab* plane resistance of the single-crystal sample. In our high-pressure ac susceptibility measurements, the sample is surrounded by a secondary coil (pickup coil) and a field-generating primary coil is wound on top of the secondary coil. The alternating flux through the pickup coil produces an ac voltage which is the measured signal. When the sample is cooled below T_C, the field is expelled from the sample due to the superconducting shielding effect, forcing some of the flux lines out of the pickup coil and leading to a reduction in the induced voltage in the pickup coil [22–25]. A lock-in amplifier (SR830) is used to generate an ac magnetic field through the primary coil and to detect the drop in the induced voltage through the secondary coil. The frequency used for the χ' data is 217 Hz, and the primary coil yields a magnetic field of 3 Oe at this frequency. The balanced secondary coils are connected with a lock-in amplifier. In order to minimize this temperature-dependent background, we used a high-pressure cell made from a Be-Cu alloy to generate pressure and a Be-Cu sheet as a gasket, because the Be-Cu alloy is a nonmagnetic material. Even so, we first measured the ac susceptibility for the high-pressure cell, without a sample but with coils and gaskets, to get the background, and then performed the ac susceptibility measurement for the sample in the same high-pressure cell. To pick up the signal from the sample carefully, we did the background subtraction.

High-pressure x-ray diffraction (XRD) measurements were performed at room temperature on beamline 15U at the Shanghai Synchrotron Radiation Facility and beamline 4W2 at the Beijing Synchrotron Radiation Facility. Diamonds with low birefringence were selected for these XRD measurements. A monochromatic x-ray beam with a wavelength of 0.6199 Å was employed and silicon oil served as a pressure-transmitting medium [26–28].

The high-pressure heat capacity of the sample under pressure was derived from ac calorimetry. Pressure is determined by the pressure dependence of T_C of Pb [29] that is placed together with the sample in a Teflon capsule. In this technique, a small temperature oscillation ΔT generated by a heater glued to one face of the crystal is converted to an ac voltage signal by a chromel-AuFe (0.07%) thermocouple fixed on the opposite side and $C \propto 1/T$. The pressure for all measurements in a diamond-anvil cell was determined by the ruby fluorescence method [30].

III. RUSULTS AND DISCUSSIONS

High-pressure heat capacity measurements down to 4 K reveal two anomalies that, like CeIrGe$_3$ [4], are associated with antiferromagnetic (AFM) transitions (see Fig. 1). We denote the higher AFM transition as T_{N1} and the lower one by T_{N2}. These two AFM transitions at T_{N1} and T_{N2} are identified from our high-pressure resistance measurements and the minima in second derivatives of the resistivity (Figs. 2 and 3). Figure 2(a) shows temperature dependence of resistance for CeRhGe$_3$ at ambient pressure, from which T_{N1} and T_{N2} can be observed (as indicated by arrows in the inset of the figure). With increasing pressure, T_{N1} and T_{N2} move to higher temperatures [Figs. 2(b) and 3(a)], consistent with the previously reported pressure dependence of T_{N1} [15]. T_{N1} reaches a maximum at 8.5 GPa and T_{N2} is maximized near 10.5 GPa. Both transitions decrease at higher pressures and merge at ~13.7 GPa within experimental resolution. This is seen most clearly in the pressure evolution of $\partial^2 R/\partial T^2$ shown in Fig. 3(a). The merged AFM transition temperature T_N falls monotonically with increasing pressure up to 18.6 GPa [Figs. 2(c) and 3(b)]. This merging and the pressure dependence of two antiferromagnetic transitions are similar to that reported for CeIrGe$_3$ [12]. At 20.5 GPa, we found a resistive drop at ~1 K [inset of Fig. 2(c)]. To investigate the new resistive drop, we carried out a new experimental run [Fig. 2(d)]. It is seen that, at 19.6 GPa where $T_N = 3.6\,\mathrm{K}$ [as indicated by the arrow in the inset of Fig. 2(d)], there is a pronounced drop in resistance at ~1.1 K. This resistance drop is largest at 21.5 GPa, where the resistance declines by ~76.6%, and then the drop becomes smaller upon further compression [Fig. 2(d)]. This observation is confirmed in a separate measurement in which a pressure-induced resistance drop is ~92.8% at 22.0 GPa, as shown in Fig. 2(f). To explore the origin of this resistance drop, we applied a magnetic field to CeRhGe$_3$ subjected to 21.5 GPa and cooled the high-pressure cell to 40 mK. As shown in Fig. 2(e) the onset temperature of the resistance drop shifts to a lower temperature upon increasing magnetic field. Furthermore, ac susceptibility measured at 20.1 GPa [the inset of Fig. 2(e)] becomes diamagnetic at ~1.2 K. All these measurements show that the pressure-induced resistance drop in low temperatures results from a superconducting transition.

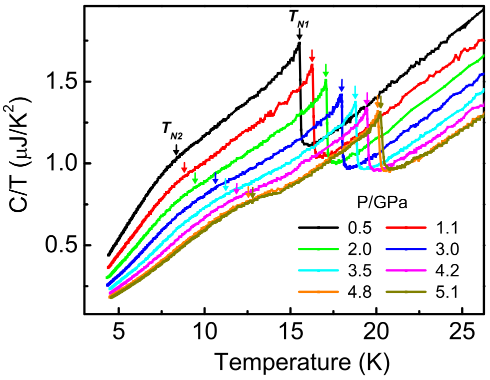

FIG. 1. Temperature dependences of heat capacity divided by temperature (C/T) at different pressures. T_{N1} and T_{N2} correspond to the higher and lower AFM transition temperatures, respectively.

To know the superconducting volume in our sample, we used the same high-pressure cell and the gasket to perform the susceptibility measurement on lead (Pb) which is considered to have 100% superconducting volume. It is found that the voltage drop from Pb in the pickup coil is about 28 nV. Consequently, we can estimate the superconducting volume of our sample that is subjected to 20.1 GPa and its superconductivity coexists with AFM order to be about 11%. Based on these results, we propose that the superconductivity at 20.1 GPa is likely a filamentarylike superconductivity, in good agreement with a body of evidence in correlated electron materials that filamentarylike superconductivity develops above the bulk superconducting transition when antiferromagnetic order is present and that the resistive T_C nearly coincides with the bulk T_C once evidence

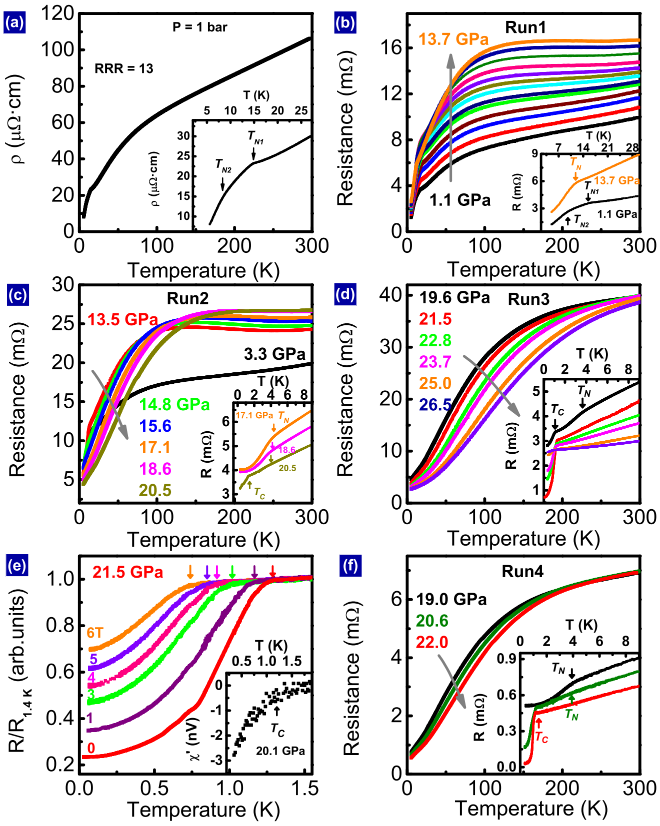

FIG. 2. High-pressure electrical resistance and ac susceptibility of CeRhGe$_3$. (a) Temperature dependence of resistivity for the ambient-pressure CeRhGe$_3$ sample investigated in this study. Residual resistivity ratio (RRR) of our sample is about 13, similar to the result (RRR = 15) reported in Ref. [7]. (b) The temperature dependence of resistance at pressures from 1.1 to 13.7 GPa. The pressures are 1.1, 2.2, 3.4, 4.2, 5.4, 6.3, 7.6, 8.5, 9.3, 10.4, 11.4, 12.7, and 13.7 GPa from the bottom to the top. The inset displays evidence for two antiferromagnetic transition temperatures, T_{N1} and T_{N2} (as indicated by arrows), for $P = 1.1$ GPa that merge together at 13.7 GPa (as indicated by orange arrow). (c) The temperature dependence of resistance for another run in the pressure range of 3.3–20.5 GPa. The inset is an enlarged view of the resistance in the lower-temperature regime, showing only one AFM transition at 17.1 and 18.6 GPa, and another resistance drop at low temperatures at 20.5 GPa. (d) The temperature dependence of resistance obtained in the pressure range of 19.6–26.5 GPa. The inset is an enlarged view of the resistance in the lower-temperature regime. As discussed in the text, the pronounced drop in resistance at low temperatures reflects a pressure-induced superconducting transition. (e) The temperature dependence of the normalized resistance measured at 21.5 GPa under different magnetic fields. The arrows indicate the onset temperature of the superconducting transition. The inset displays the real part of ac susceptibility measured at 20.1 GPa. (f) The resistance versus temperature measured in another run where the resistance drop at T_C is more pronounced.

for magnetic order is absent [31,32]. Note that the resistance below the onset temperature is still finite which is possibly due to the presence of sample microcracks generated by the quasihydrostatic pressure environment.

We extract the field dependence of T_C for CeRhGe$_3$ at 21.5 GPa [Fig. 2(e)] and display it in Fig. 4. We did a linear fit for the magnetic dependence of T_C (as shown by the dashed line in Fig. 4). The rate of decrease of the onset temperature is very high (–11.6 T/K), a huge value that a characteristic of the weak temperature dependence of the magnetic field of pressure-induced superconductivity in other CeTX_3 compounds [5]. Extrapolation of the linear fit to zero temperature yields upper critical pressure about 15 T at 21.5 GPa.

This pressure-induced superconductivity emerges in the noncentrosymmetric $I4mm$ crystal structure. Results of synchrotron x-ray diffraction (XRD) measurements on CeRhGe$_3$ at pressures up to 28.5 GPa are summarized in Fig. 5. With increasing pressure, the lattice constants decrease, but the crystal structure remains unchanged. A fit of the pressure-dependent cell volume to a Murnaghan equation of state ($V = V_0[1 + P(B'/B)]^{-1/B'}$) gives a bulk modulus ($B$) and its pressure derivative (B') of 115 GPa and 5, respectively. Here B is the isothermal bulk modulus at zero pressure, B' is the pressure derivative of B evaluated at zero pressure, and V and V_0 are the high-pressure volume and zero-pressure volume of the material, respectively. The stability of the structure against pressure rules out the possibility that the superconductivity emerges in a different crystal structure at low temperatures. This is consistent with the observation of the huge $\partial H_{C2}/\partial T$ of CeRhGe$_3$ which is a common feature of these noncentrosymmetric superconductors.

Figure 6 shows the pressure-temperature phase diagram obtained from our measurements. The overall bell-shaped response of antiferromagnetism to applied pressure is captured in Doniach's model of competing Ruderman-Kittel-Kasuya-Yosida (RKKY) and Kondo interactions [33]. With increasing pressure, the Kondo hybridization becomes dominant, which suppresses the RKKY-mediated long-range order. However, T_N does not go continuously to zero temperature. A similar pressure dependence of the AFM transition temperature is also found in CeIrGe$_3$ [12]. Nevertheless, the substantially suppressed Néel order around 20 GPa leaves the possibility that magnetic fluctuations could play a role in inducing superconductivity that initially coexists with antiferromagnetic order.

In Fig. 7(a) we place our discovery of superconductivity in CeRhGe$_3$ in the context of early results on other members of the CeTX_3 family [4–13,15,18] and compare the pressure dependence of the superconducting transition temperature for the whole CeTX_3 family. We find that the critical pressure P_{crit} at which pressure-induced superconductivity reaches a maximum T_C is strongly correlated with the unit-cell volume at the ambient pressure [Fig. 7(a)]. For X = Si or Ge, the cell volume increases in the sequence T = Co, Rh, Ir, and for a given T, the cell volume is larger for X = Ge. CeCoSi$_3$, with the smallest cell volume, has a mixed-valence 4f configuration reflecting strong hybridization between f and conduction (c) electrons and is not superconducting above 0.5 K [34]. In contrast, the Kondo hybridization in the large-cell compounds, CeIrGe$_3$ and CeRhGe$_3$, is much weaker [4]. As the unit cell expands, the critical pressure P_{crit} increases by an order of magnitude from CeRhSi$_3$ to CeIrGe$_3$. This correlation implies that an optimally large hybridization and, thus, an optimally strong Kondo coupling induced by compression are required for superconductivity.

Assuming that our equation of state for CeRhGe$_3$ provides a reasonable approximation for estimating the cell volume

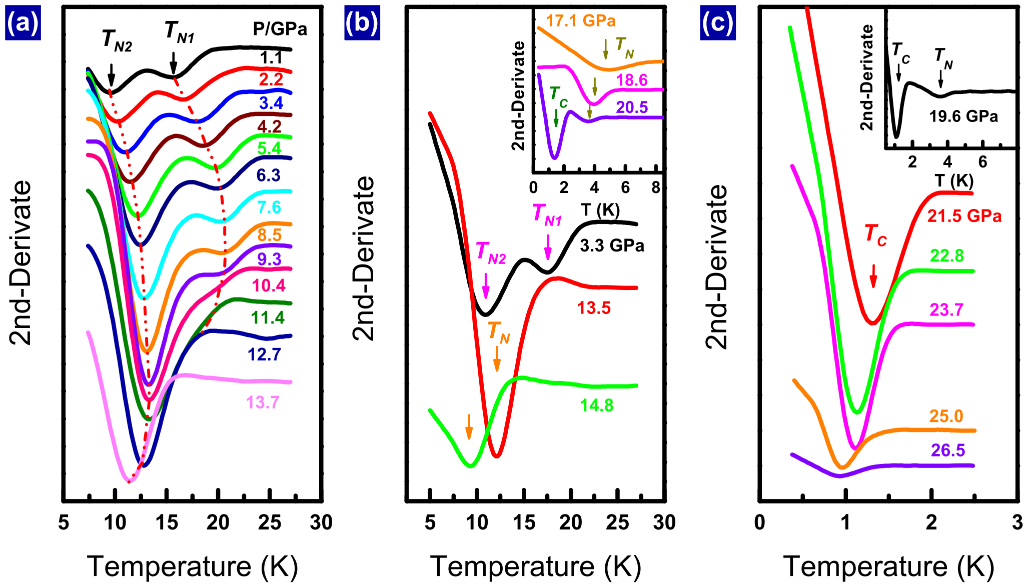

FIG. 3. Second derivate of the electrical resistance with respect to temperature for CeRhGe$_3$ crystals at different pressures. (a),(b) Pressure-induced evolution of transition temperatures T_{N1} and T_{N2} that merge into a single transition T_N. The insets of (b) display details of the second derivate in the lower-temperature range near the boundary of antiferromagnetism and superconductivity. (c) Pressure dependence of the superconducting transition temperature T_C as revealed by the second derivative of resistance.

of other CeTX_3 members at P_{crit}, we plot in Fig. 7(b) the maximum superconducting transition temperature T_C^{max} as a function of critical cell volume V_{crit} at P_{crit}. Interestingly, all T_C^{max} fall within a rather narrow range of V_{crit} values that vary by only ±1.7%, as emphasized by the vertical dashed lines in Fig. 7(a). It appears, then, that there is an approximate optimal cell volume for achieving a maximum T_C. Because all the family members are nominally isoelectronic, this correlation could be interpreted as reflecting an optimal hybridization or Kondo coupling for a maximum T_C. Further, as shown by dashed lines in Fig. 7(a), V_{crit}, and by inference a critical hybridization or Kondo coupling strength, places optimal superconductivity near the crossover to a mixed-valence regime found in CeCoSi$_3$. This raises the possibility that critical valence fluctuations also might play a role in producing superconductivity in the CeTX_3 series, with CeCoSi$_3$ being too far into the mixed-valence regime for those fluctuations to be effective.

Perhaps the most interesting correlation is that T_C^{max} increases systematically as the T element changes from $3d$ to $4d$

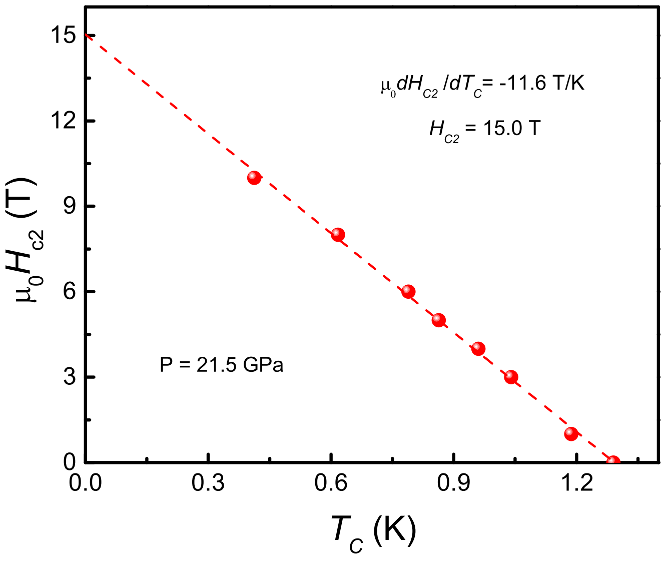

FIG. 4. Plot of superconducting transition temperature T_C versus upper critical field for CeRhGe$_3$ at 21.5 GPa. The dashed line represents a linear fit to the data.

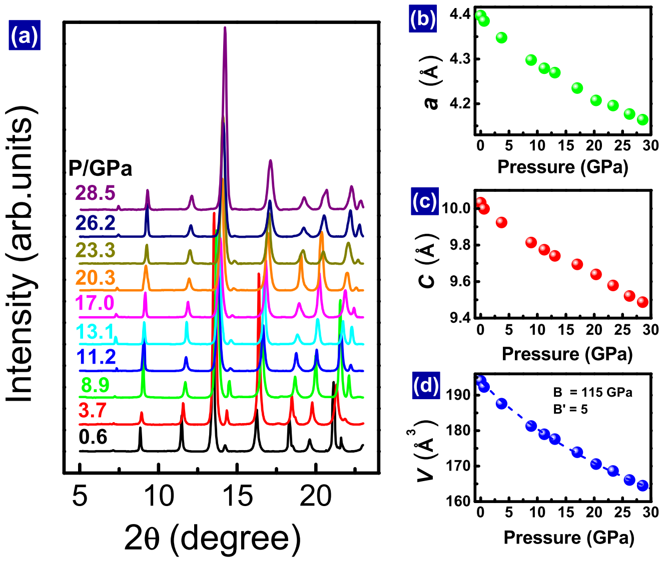

FIG. 5. Structure of CeRhGe$_3$ under pressure. (a) X-ray diffraction patterns of CeRhGe$_3$ collected at different pressures, showing no structure phase transition up to 28.5 GPa. (b)–(d) Pressure dependence of lattice parameters a, c and unit-cell volume (V). The dashed curve in (d) is a fit of data to a Murnaghan equation of state that yields a bulk modulus $B = 115$ GPa and its pressure derivative $B' = 5$.

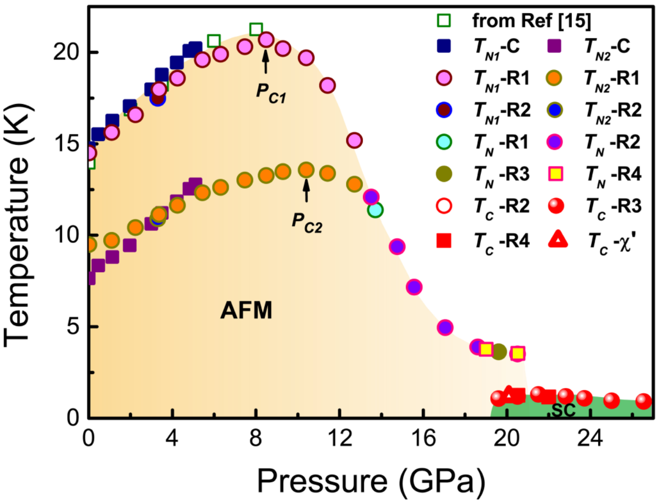

FIG. 6. Temperature-pressure phase diagram for $CeRhGe_3$. The solid squares in navy and purple represent the T_{N1} and T_{N2} transition temperatures determined by our high-pressure heat capacity measurements. The solid circles in magenta (wine) and orange (blue) represent the T_{N1} and T_{N2} transition temperatures determined by our high-pressure resistance measurements. P_{C1} and P_{C2} are the critical pressures where the T_{N1} and T_{N2} show a maximum value. The violet (cyan and dark yellow) circles and yellow squares stand for the merged antiferromagnetic transition temperature (T_N) above 13.7 GPa. The solid red circles, squares, open circles, and open triangle denote the superconducting transition temperature (T_C) determined by high-pressure resistance and ac susceptibility measurements. The olive squares are T_{N1} transition temperatures adopted from Ref. [15].

to $5d$, and for T = Rh and Ir, $T_C^{\max}$ is similar irrespective of the X element. With a fixed angular momentum of the T elements, the atomic spin-orbit interaction strength, which gives rise to a Rashba antisymmetric spin-orbit coupling [6], is proportional to Z^4/n^3, where Z is the atomic number and n is the principal quantum number. Normalizing this ratio to 1 for T = Co, then the atomic spin-orbit coupling is ∼3 and ∼14 times stronger for T = Rh and Ir, respectively. The observation that $T_C^{\max}$ is comparable for T = Rh and Ir irrespective of X suggests that spin-orbit coupling of the X elements may not play such an important role, and, indeed, X elements tend to act as "inert" spacers. As an aside, we note that of all the members, $CeCoGe_3$ is the only one with a magnetic easy plane, as opposed to others with an easy axis [7], and $CeCoSi_3$ is strongly hybridized. The clear correlation in Fig. 7(b) is that $T_C^{\max}$ increases with increasing spin-orbit coupling strength.

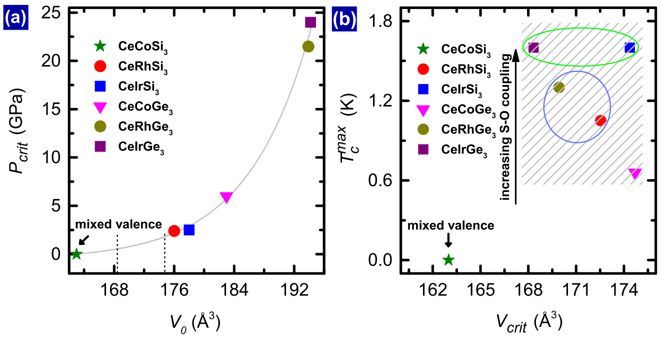

FIG. 7. Correlations among $CeTX_3$ ambient-pressure cell volume, critical pressure P_{crit} for developing a maximum superconducting transition $T_C^{\max}$ and cell volume at $T_C^{\max}$. (a) Critical pressure where T_C reaches its maximum value as a function of ambient-pressure unit-cell volume V_0. The vertical dashed lines along the abscissa reflect the range of volumes marked by the hashed box in (b). (b) Plot of maximum T_C versus unit-cell volume V_{crit} where a maximum T_C is observed. The critical volume for superconducting $CeRhGe_3$ is determined from the equation of state [Fig. 5(d)]: $V_{\mathrm{crit}} = V_0[1 + P_{\mathrm{crit}}(B'/B)]^{-1/B'}$ with $B = 115\,\mathrm{GPa}$ and $B' = 5$. We assume this same relationship to estimate V_{crit} for other family members.

The role of antisymmetric spin-orbit coupling is to lift spin degeneracy of single-particle states, removing parity symmetry and creating spin-split electronic bands in which spins are polarized tangential to the electrons' momentum. In general, band splitting due to antisymmetric spin-orbit coupling is band dependent, and an effective antisymmetric spin-orbit coupling is expected to depend on the extent of hybridization between f and conduction electrons [35]. Though a correlation between $T_C^{\max}$ and magnitude of the atomic spin-orbit coupling is obvious in Fig. 7(b), the correlation is not 1:1 because f-c hybridization, and hence effective antisymmetric spin-orbit coupling, varies with the T element. From results in Fig. 7, we conclude, then, that spin-orbit coupling is a key factor in determining the maximum value of T_C in the $CeTX_3$ family and that a narrow range of cell volumes, i.e., hybridization, is necessary for inducing a superconducting state.

IV. CONCLUSION

We have discovered superconductivity in heavy-fermion $CeRhGe_3$, the last nonsuperconducting member of the $CeTX_3$ family. This discovery has allowed an alternative perspective on conditions necessary for superconductivity in the family and for the maximum T_C that its members reach. It is not possible from our studies to make definitive statements about the pairing mechanism or symmetry of the superconducting pairs, but it seems that magnetic as well as valence fluctuations could be effective in Cooper pairing and that, with higher maximum T_C's in the sequence $X = 3d$, $4d$ to $5d$, spin-orbit coupling plays a progressively dominant role in determining the gap symmetry. Clearly, this work calls for new experiments to determine the evolution of the relative admixture of spin-singlet and spin-triplet pairing across the series, to search for evidence of valence and magnetic fluctuations in the vicinity of V_{crit}, and for theory that explicitly considers antisymmetric spin-orbit coupling, not only for its effect on the pairing symmetry but also as an initial condition for superconductivity in $CeTX_3$ materials and in noncentrosymmetric compounds more broadly.

ACKNOWLEDGMENTS

We thank Professor Frank Steglich for helpful discussions. The work in China was supported by the National Key Research and Development Program of China (Grants No. 2017YFA0303103, No. 2017YFA0302900, No. 2016YFA0300300, and No. 2015CB921303), the

NSF of China (Grants No. 11427805, No. U1532267, No. 11604376, and No. 11522435), and the Strategic Priority Research Program (B) of the Chinese Academy of Sciences (Grant No. XDB07020300). Work at Los Alamos National Laboratory was performed under the auspices of the U.S. DOE, Office of Basic Energy Sciences, Division of Materials Sciences and Engineering.

H.W. and J.G. contributed equally to this work.

[1] F. Steglich, J. Aarts, C. D. Bredl, W. Lieke, D. Meschede, W. Franz, and H. Schäfer, Phys. Rev. Lett. **43**, 1892 (1979).
[2] C. Pfleiderer, Rev. Mod. Phys. **81**, 1551 (2009).
[3] P. Haen, P. Lejay, B. Chevalier, B. Lloret, J. Etourneau, and M. Sera, J. Less-Common Met. **110**, 321 (1985).
[4] Y. Muro, D. Eom, N. Takeda, and M. Ishikawa, J. Phys. Soc. Jpn. **67**, 3601 (1998).
[5] N. Kimura and I. Bonalde, in *Non-Centrosymmetric Superconductors*, edited by E. Bauer and M. Sigrist (Springer, Berlin, 2012), pp. 35–79.
[6] M. Smidman, M. B. Salamon, H. Q. Yuan, and D. F. Agterberg, Rep. Prog. Phys. **80**, 036501 (2017).
[7] T. Kawai, H. Muranaka, M.-A. Measson, T. Shimoda, Y. Doi, T. D. Matsuda, Y. Haga, G. Knebel, G. Lapertot, D. Aoki, J. Flouquet, T. Takeuchi, R. Settai, and Y. Ōnuki, J. Phys. Soc. Jpn. **77**, 064716 (2008).
[8] I. Sugitani, Y. Okuda, H. Shishido, T. Yamada, A. Thamizhavel, E. Yamamoto, T. D. Matsuda, Y. Haga, T. Takeuchi, R. Settai, and Y. Ōnuki, J. Phys. Soc. Jpn. **75**, 043703 (2006).
[9] N. Kimura, K. Ito, K. Saitoh, Y. Umeda, H. Aoki, and T. Terashima, Phys. Rev. Lett. **95**, 247004 (2005).
[10] R. Settai, Y. Okuda, I. Sugitani, Y. Ōnuki, T. D. Matsuda, Y. Haga, and H. Harima, Int. J. Mod. Phys. B **21**, 3238 (2007).
[11] G. Knebel, D. Aoki, G. Lapertot, B. Salce, J. Flouquet, T. Kawai, H. Muranaka, R. Settai, and Y. Ōnuki, J. Phys. Soc. Jpn. **78**, 074714 (2009).
[12] F. Honda, I. Bonalde, K. Shimizu, S. Yoshiuchi, Y. Hirose, T. Nakamura, R. Settai, and Y. Ōnuki, Phys. Rev. B **81**, 140507(R) (2010).
[13] N. Kimura, K. Ito, H. Aoki, S. Uji, and T. Terashima, Phys. Rev. Lett. **98**, 197001 (2007).
[14] R. Settai, Y. Miyauchi, T. Takeuchi, F. Lévy, I. Sheikin, and Y. Ōnuki, J. Phys. Soc. Jpn. **77**, 073705 (2008).
[15] T. Kawai, M. Nakashima, Y. Okuda, H. Shishido, T. Shimoda, T. D. Matsuda, Y. Haga, T. Takeuchi, M. Hedo, Y. Uwatoko, R. Settai, and Y. Ōnuki, J. Phys. Soc. Jpn. **76**, 166 (2007).
[16] T. Sugawara, H. Iida, H. Aoki, and N. Kimura, J. Phys. Soc. Jpn. **81**, 054711 (2012).
[17] J. F. Landaeta, D. Subero, D. Catalá, S. V. Taylor, N. Kimura, R. Settai, Y. Ōnuki, M. Sigrist, and I. Bonalde, arXiv:1702.06812.
[18] N. Kimura, Y. Muro, and H. Aoki, J. Phys. Soc. Jpn. **76**, 051010 (2007).
[19] N. N. Zhuravlev and G. S. Zhdanov, Sov. Phys. Crystallogr. **1**, 158 (1956).
[20] H. Okamoto, in *Binary Alloy Phase Diagrams*, 2nd ed., edited by T. B. Massalski, H. Okamoto, P. R. Subramanian, and L. Kacprzak (ASM International, Materials Park, OH, 1990), Vol. 2, pp. 1989–1991.
[21] G. J. Piermarini, S. Block, and J. D. Barnett, J. Appl. Phys. **44**, 5377 (1973).
[22] V. G. Tissen, E. G. Ponyatovskii, M. V. Nefedova, F. Porsch, and W. B. Holzapfel, Phys. Rev. B **53**, 8238 (1996).
[23] J. J. Hamlin, V. G. Tissen, and J. S. Schilling, Phys. Rev. B **73**, 094522 (2006).
[24] M. Debessai, J. J. Hamlin, and J. S. Schilling, Phys. Rev. B **78**, 064519 (2008).
[25] L. L. Sun, X.-J. Chen, J. Guo, P. W. Gao, Q.-Z. Huang, H. D. Wang, M. H. Fang, X. L. Chen, G. F. Chen, Q. Wu, C. Zhang, D. C. Gu, X. L. Dong, L. Wang, K. Yang, A. G. Li, X. Dai, H.-K. Mao, and Z. X. Zhao, Nature (London) **483**, 67 (2012).
[26] D. D. Ragan, D. R. Clarke, and D. Schiferl, Rev. Sci. Instrum. **67**, 494 (1996).
[27] Y. Shen, R. S. Kumar, M. Pravica, and M. F. Nicol, Rev. Sci. Instrum. **75**, 4450 (2004).
[28] N. Tateiwa and Y. Haga, Rev. Sci. Instrum. **80**, 123901 (2009).
[29] A. Eiling and J. S. Schilling, J. Phys. F: Met. Phys. **11**, 623 (1981).
[30] H. K. Mao, J. Xu, and P. M. Bell, J. Geophys. Res. **91**, 4673 (1986).
[31] T. Park, H. Lee, I. Martin, X. Lu, V. A. Sidorov, K. Gofryk, F. Ronning, E. D. Bauer, and J. D. Thompson, Phys. Rev. Lett. **108**, 077003 (2012).
[32] T. Park, X. Lu, H.-O. Lee, and J. D. Thompson, Phys. C (Amsterdam, Neth.) **481**, 223 (2012).
[33] S. Doniach, Physica B+C (Amsterdam) **91**, 231 (1977).
[34] T. Shimoda, Y. Okuda, Y. Takeda, Y. Ida, Y. Miyauchi, T. Kawai, T. Fujie, I. Sugitani, A. Thamizhavel, T. D. Matsuda, Y. Hagab, T. Takeuchic, M. Nakashima, R. Settai, and Y. Ōnuki, J. Magn. Magn. Mater **310**, 308 (2007).
[35] H. Iida, Y. Kadota, M. Kogure, T. Sugawara, H. Aoki, and N. Kimura, J. Phys. Soc. Jpn. **80**, 083701 (2011).